

MAGNETISM
II – MATERIALS AND APPLICATIONS

edited by

Étienne du TRÉMOLET de LACHEISSERIE
Damien GIGNOUX
Michel SCHLENKER

Grenoble Sciences
2002

AUTHORS

- Michel CYROT** - Professor at the Joseph Fourier University of Grenoble, France
- Michel DÉCORPS** - Senior Researcher, INSERM (French Institute of Health and Medical Research), Bioclinical Magnetic Nuclear Resonance Unit, Grenoble
- Bernard DIÉNY** - Researcher and group leader at the CEA (French Atomic Energy Center), Grenoble
- Etienne du TRÉMOLET de LACHEISSERIE** - Senior Researcher, CNRS, Laboratoire Louis Néel, Grenoble
- Olivier GEOFFROY** - Assistant Professor at the Joseph Fourier University of Grenoble
- Damien GIGNOUX** - Professor at the Joseph Fourier University of Grenoble
- Ian HEDLEY** - Researcher at the University of Geneva, Switzerland
- Claudine LACROIX** - Senior Researcher, CNRS, Laboratoire Louis Néel, Grenoble
- Jean LAFOREST** - Research Engineer, CNRS, Laboratoire Louis Néel, Grenoble
- Philippe LETHUILLIER** - Engineer at the Joseph Fourier University of Grenoble
- Pierre MOLHO** - Researcher, CNRS, Laboratoire Louis Néel, Grenoble
- Jean-Claude PEUZIN** - Senior Researcher, CNRS, Laboratoire Louis Néel, Grenoble
- Jacques PIERRE** - Senior Researcher, CNRS, Laboratoire Louis Néel, Grenoble
- Jean-Louis PORTESEIL** - Professor at the Joseph Fourier University of Grenoble
- Pierre ROCHETTE** - Professor at the University of Aix-Marseille 3, France
- Michel-François ROSSIGNOL** - Professor at the Institut National Polytechnique de Grenoble (Technical University)
- Yves SAMSON** - Researcher and group leader at the CEA (French Atomic Energy Center) in Grenoble
- Michel SCHLENKER** - Professor at the Institut National Polytechnique de Grenoble (Technical University)
- Christoph SEGEBARTH** - Senior Researcher, INSERM (French Institute of Health and Medical Research), Bioclinical Magnetic Nuclear Resonance Unit, Grenoble
- Yves SOUCHE** - Research Engineer, CNRS, Laboratoire Louis Néel, Grenoble
- Jean-Paul YONNET** - Senior Researcher, CNRS, Electrical Engineering Laboratory, Institut National Polytechnique de Grenoble (Technical University)

Grenoble Sciences

"Grenoble Sciences" was created ten years ago by the Joseph Fourier University of Grenoble, France (Science, Technology and Medicine) to select and publish original projects. Anonymous referees choose the best projects and then a Reading Committee interacts with the authors as long as necessary to improve the quality of the manuscript.

(Contact : Tél. : (33)4 76 51 46 95 - E-mail : Grenoble.Sciences@ujf-grenoble.fr)

The "Magnetism" Reading Committee included the following members :

- ◆ **V. Archambault**, Engineer - Rhodia-Recherche, Aubervilliers, France
- ◆ **E. Burzo**, Professor at the University of Cluj, Rumania
- ◆ **I. Campbell**, Senior Researcher - CNRS, Orsay, France
- ◆ **F. Claeyssen**, Engineer - CEDRAT, Grenoble, France
- ◆ **G. Couderchon**, Engineer - Imphy Ugine Précision, Imphy, France
- ◆ **J.M.D. Coey**, Professor - Trinity College, Dublin, Ireland
- ◆ **A. Fert**, Professor - INSA, Toulouse, France
- ◆ **D. Givord**, Senior Researcher - Laboratoire Louis Néel, Grenoble, France
- ◆ **L. Néel**, Professor, Nobel Laureate in Physics, Member of the French Academy of Science
- ◆ **B. Raquet**, Assistant Professor - INSA, Toulouse, France
- ◆ **A. Rudi**, Engineer - ECIA, Audincourt, France
- ◆ **Ph. Tenaud**, Engineer - UGIMAG, St-Pierre d'Allevard, France

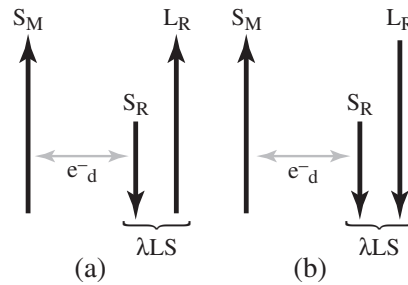
"Magnetism" (2 volumes) is an improved version of the French book published by "Grenoble Sciences" in partnership with EDP Sciences with support from the French Ministry of Higher Education and Research and the "Région Rhône-Alpes".

EXTRAITS

6.3.2. R-M coupling = ferromagnetism or ferrimagnetism

The antiparallel coupling between spin moments of M and R atoms combines with spin-orbit coupling at the R site (see fig. 15.54). S_M is coupled to S_R by exchange via a d electron, and S_R is coupled to L_R via spin-orbit coupling.

Figure 15.54 - Relative arrangement of magnetic moments in R-M compounds
 (a) R = light rare earth (1st series)
 (b) R = heavy rare earth (2nd series)
 The coupling is indicated in grey.



For heavy rare earth elements (from Tb to Tm), L and S are parallel, and the total moments of M and R are antiparallel. For the light rare earth elements (Pr, Nd and Sm), L and S are antiparallel, and $L\mu_B > 2S\mu_B$, so that the total moments of M and R are parallel. This ferromagnetic coupling is the basis for the fact that, within a given series of compounds, the magnetization is stronger in those compounds involving light rare earths (see fig. 15.55, and, as an example, the magnetization of RCO_5 or $R_2Fe_{14}B$ compounds in fig. 15.56).

Figure 15.55 - Resultant magnetic moment for three RCO_5 compounds

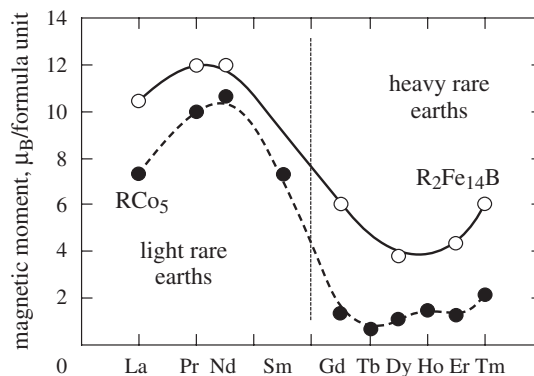
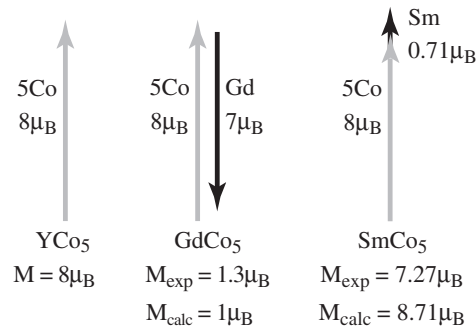


Figure 15.56 - Magnetic moments of RCO_5 , and $R_2Fe_{14}B$ compounds

Figure 16.20 illustrates the effect of the correlation length of the random medium, and shows how two opposed strategies lead to very soft materials. One consists in averaging the fluctuations at very short scale, 10 nm in nanocrystalline materials, less than 1 nm in amorphous metals. On the contrary, the largest grains give lower coercive fields in classical crystalline materials.

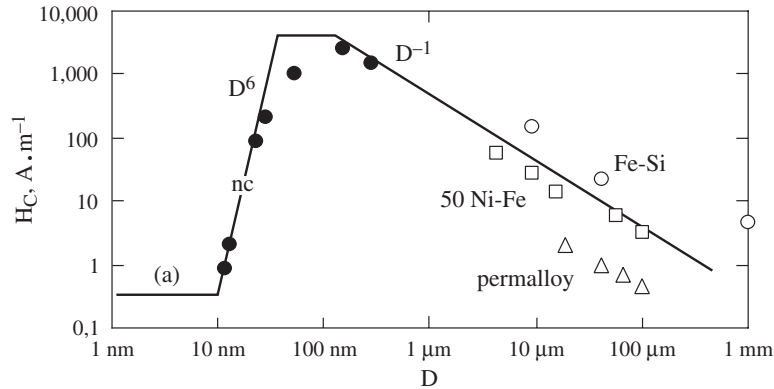


Figure 16.20 - Coercive field (H_c) as a function of the grain size (D) for different families of soft materials (after [21])

Amorphous (a), nanocrystallized (nc) and crystallized materials (Fe-Si, 50FeNi and Permalloy)

6.3. APPLICATIONS OF NANOCRYSTALLINE MATERIALS

Their high permeability and their weak energy loss in ac regime (see tab. 16.7) make them valuable for safety devices (differential circuit breakers), sensors, high frequency transformers (at least up to 100 kHz), filtering inductances... The possibility to play with the value and the direction of the uniaxial anisotropy gives nanocrystalline alloys the same versatility as Fe-Ni-Mo crystallized materials or cobalt rich amorphous metals. With respect to the latter, they exhibit the advantages of a larger polarization, and of good thermal stability of their characteristics thanks to a relatively high Curie temperature of the Fe-Si phase, as well as a probably better time stability. On the other hand they are very brittle.

Table 16.7 - Main characteristics of a nanocrystalline material with typical composition $Fe_{73.5}Cu_1Nb_3Si_{13.5}B_9$

B_s (T)	H_c (A.m ⁻¹)	μ_r^{max} (DC)	μ_r^{max} (50 Hz)	μ_r^{max} (1 kHz)	L (W.kg ⁻¹)
1.25	0.5	$> 8 \times 10^5$	$> 5 \times 10^5$	10^5	40

The losses L are measured at 100 kHz and in 0.2 tesla.

Nanocrystalline alloys with other compositions are still laboratory materials but they could become attractive for applications thanks to their large saturation polarization.

$$R_m = \omega \mu''_e \mu_0 n^2 S / l = L \omega / Q_e,$$

where Q_e is the effective quality factor defined above. Finally, the quality factor of the inductance can be expressed as:

$$Q = L\omega / [R_1 / \mu'_e + L\omega / Q_e] = 1 / [(\mu'_e Q_1)^{-1} + \mu'_e / M_e] \quad (17.114)$$

where M_e is the figure of merit, and $Q_1 = L\omega / R_1$.

We see that as μ'_e is altered at constant M_e (by acting on the air gap ratio g/l), the quality factor Q goes through a maximum when:

$$\mu'_e = \mu_{opt} = (M_e / Q_1)^{1/2} \quad (17.115)$$

We note that this corresponds to $R_m = R_1 / \mu'_e = R_2$, hence to equal contributions to the losses from the copper and the magnetic material.

The maximum value of the quality factor is $Q = (1/2)(Q_1 M_e)^{1/2} = Q_e / 2 = Q_2 / 2$, where $Q_2 = L\omega / R_2$. A numerical example is given in Exercise 4 at the end of this chapter.

7. OVERVIEW OF MICROWAVE MATERIALS AND APPLICATIONS

The materials used for microwave technology (tab. 17.4) are described in detail by Von Aulock [29], and more recently by Nicolas [35]. The spinels and hexaferrites, which we very partly described in section 6, are complemented by the ferrimagnetic garnets, discovered in Grenoble at the end of the 1950's by Bertaut and Forrat [36].

Table 17.4 - Main materials used in microwave technology

Spinel	(Mg-Zn) Fe ₂ O ₄ , (Mn-Zn)Fe ₂ O ₄ , (Ni -Zn) Fe ₂ O ₄ , Li _{0,5} Fe _{2,5} O ₄
Hexaferrites	type M: Ba Fe ₁₂ O ₁₉ and substituted (easy axis) type Y, Z (easy plane)
Garnets	YIG: Y ₃ Fe ₅ O ₁₂ , (Ga, Al, Cr, In, Sc) substituted YIG and rare-earth (La, Pr, Nd, Sm, Eu, Gd, Tb, Dy, Ho, Er, Yb, Lu) substituted YIG

7.1. THE FERRIMAGNETIC GARNETS

The basic formula of the ferrimagnetic garnets is $R_3Fe_5O_{12}$ where R is a rare-earth element (with a restriction, however, on the ionic radius –see ref. [29]) or yttrium. These compounds crystallise in the cubic system, but their structure is much more complicated than for spinels. They are described in reference [29], which also provides a rather complete description of the chemical, structural and magnetic properties of this family, which turns out to be extremely rich when the many possible substitutions to the basic formula are taken into account.

Among all these compounds, yttrium iron garnet $\text{Y}_3\text{Fe}_5\text{O}_{12}$, usually designated by the acronym YIG, plays a dominant role because its rotation damping is particularly small, which leads to very narrow gyromagnetic resonance lines.

The resonance is normally investigated on spheres obtained from a ceramic or from a bulk crystal, by operating at fixed excitation frequency and varying the static polarising field. This simplifies the problem both of the generation of the excitation signal and of the microwave circuitry (actually, this is a bit less true now, with the advent of digital network analysers).

The sphere can be placed in a waveguide closed by a shorting piston at distance d (close to half the wavelength) from it, and one measures the reflection coefficient (fig. 17.19). Its variation vs polarising field H in the neighbourhood of resonance takes the shape of an absorption peak, with a width at half maximum ΔH that characterises the damping. In YIG at 9 GHz, values of $\mu_0\Delta H$ on the order of 0.3 mT in ceramics and 0.03 mT in single crystals are frequently encountered.

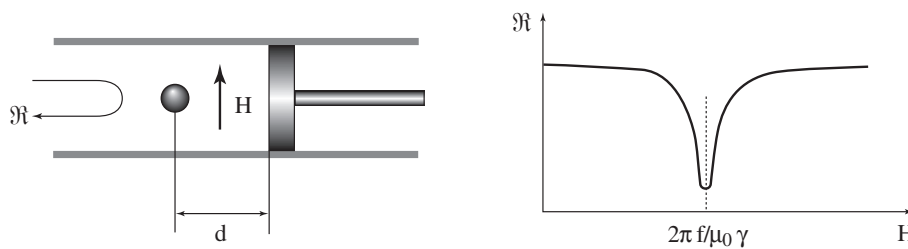


Figure 17.19 - Measuring the width of the uniform resonance line on ferrite spheres

It is often more significant to characterise the resonance through its *quality factor* $H/\Delta H$, where H is the resonance field at the frequency used. Knowing that, for YIG, $\gamma = 28 \text{ GHz/T}$, we obtain, for $f = 9 \text{ GHz}$, $\mu_0 H = 0.35 \text{ T}$ whence $Q \sim 1,000$ for ceramics and $Q \sim 10,000$ for single crystals. These high values of the quality factor are absolutely essential in the applications to filters and oscillators which we describe below.

7.2. MICROWAVE APPLICATIONS

The so-called non-reciprocal devices are the most specific, and also the most classical application of ferrites in the microwave range. They are described by Waldron [4]. We discuss them briefly here, and also describe a more recent application, the YIG resonator.

7.2.1. Non-reciprocal devices

All these devices use the gyrotropy of magnetised ferrites, i.e. the difference between the circular permeabilities μ_+ and μ_- . Here we just illustrate the principles by first

depend on the shape of the active element if the frequency becomes higher than a characteristic frequency f_c , which, for a cylinder of diameter d and electrical conductivity γ , is given by:

$$f_c = 2/(\gamma\pi\mu_{33}^\epsilon d^2) \quad (18.1)$$

where μ_{33}^ϵ is the magnetic permeability at constant deformation. The use of a composite of low electrical resistivity is then recommended.

In conclusion, at room temperature, Terfenol-D is comparable with ceramic PZT because of its strong saturation deformation and its high power density. Moreover, for low frequency applications, the lower velocity of sound (2,450 m.s⁻¹ for Terfenol-D compared to 3,100 m.s⁻¹ for PZT) allows resonance to be achieved with shorter bars. It is also better than electrostrictive materials such as PMN-PT, the good performance of which disappears at 40°C (their Curie temperature).

The principal disadvantages of Terfenol-D seem to be its hysteresis, a relative sensitivity to temperature, the necessity of magnetically polarising them and their high cost; finally we mention the fragility of the stoichiometric alloy under traction. The remedy is to hold the samples under compression and to remain slightly under-stoichiometric in iron: this is why the composition of alloys available on the market is Tb_{0.3}Dy_{0.7}Fe_x with x varying from 1.90 to 1.95 without a great variation in magnetostrictive performance.

2.3. USE OF TERFENOL-D IN ACTUATORS

Owing to their strong magnetostriction, Terfenol-D alloys are able to produce significant force, and generate rapid, precise movement with considerable power. The main industrial applications of Terfenol-D are linear actuators, which in essence are magnetostrictive bars, polarised by a static magnetic field, and usually submitted to a compressive stress, which elongate under the influence of a quasi-static or dynamic excitation field.

Some concrete examples will illustrate the precautions to be taken in selecting the most appropriate material for a given application: electro-valves (fuel injection, cryogenic applications...), micro-pumps (heads of ink jet printers), automatic tool positioning with wear compensation (machine tools), active vibration damping, fast relays, gears, auto-locking actuators (robotics), rapid shutters, automatic focusing (optics), hooping under field (when a bar of Terfenol-D elongates, its diameter decreases). More detailed information can be obtained in a recently published reference book [7].

2.3.1. Linear actuator

An example of a linear actuator is shown in figure 18.4. We see here how much the magnetic and mechanical aspects intimately overlap: it is thus best to design the entire system so as to optimise performance. Software has been developed for this purpose.

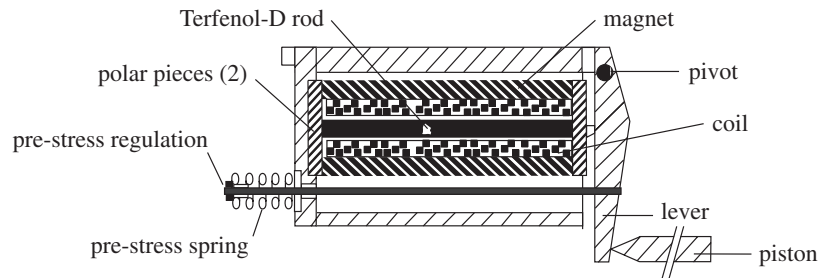


Figure 18.4 - An example of a linear actuator
(Documentation Etrema Products, Ames, IA, USA)

2.3.2. Differential actuator

Another prototype, the differential actuator, deserves to be mentioned because starting from two rectilinear movements, it can produce rotational motion of the mobile axis (fig. 18.5).

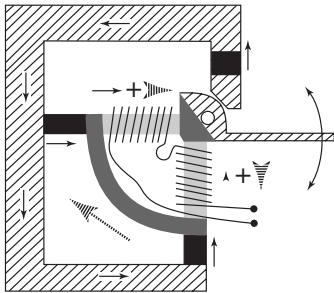


Figure 18.5 - Differential actuator

Static flux is shown by black arrows, dynamic flux by the hashed arrows. Soft magnetic material: hashed volumes; Terfenol-D bar: in light grey (under coils); magnets: in black; insulating soft magnetic materials: in dark grey [8].

Nevertheless, the motion is very restricted. The static (polarization) and dynamic (excitation) magnetic fluxes follow different paths, so it is possible to observe, in two bars placed at right angles, a dynamic magnetic field which reinforces the static field for one bar and opposes the magnetic field for the other. Thus, the first bar elongates while the second shortens, which generates the desired rotational motion.

To allow magnetostrictive bars to remain permanently under stress, it is also possible to use two aligned bars which work symmetrically: when the first elongates, the second shortens. This “push-pull” assembly is particularly well adapted to active position control since, after expansion, one of the two elements is always returned to its contracted position by the other which then expands.

2.3.3. Wiedemann effect actuators

Another very particular type of actuator exploits the direct Wiedemann effect: it consists of a spiral spring made from a magnetostrictive wire which is coated by a winding which allows it to be longitudinally magnetised.

When a current circulates in the spring, the latter is submitted to a helical magnetic field (see § 5 of chapter 12), and experiences a twisting due to the Wiedemann effect,

6.4. VORTEX PINNING

Creating a vortex requires energy since it is necessary to destroy superconductivity in a tube of radius ξ . If there is an inclusion consisting of a material which does not become superconductor, and if the vortex crosses this inclusion, its energy will be decreased since superconductivity does not have to be destroyed in the inclusion.

Shifting the vortex from this position will require a current large enough to generate a force that can move it. Current can thus flow without dissipation as long as the vortex remains pinned. Actually, the whole vortex lattice has to be pinned. The principle remains the same, but calculating the current required to move the lattice, i.e. the critical current, becomes a very complex problem which we will not treat. However, we can now understand the irreversibility observed in the magnetization.

If there are defects in the superconductor, vortices do not enter easily into the superconductor under the effect of magnetic pressure because the pinning centers oppose their displacement. Conversely, once vortices are in the material, they will not easily get out when the magnetic field is decreased, and the equilibrium state will not be reached. There is thus an irreversibility of magnetization. One can link this irreversibility to the current the superconductor can carry without dissipation since both phenomena have the same origin. If ΔM is the difference between the magnetization measured in increasing field and that measured in decreasing field (fig. 19.18), we get the approximate expression:

$$I_c = 2 \Delta M / d \quad (19.30)$$

where d is the size of the sample or, for a granular sample, that of the grains.

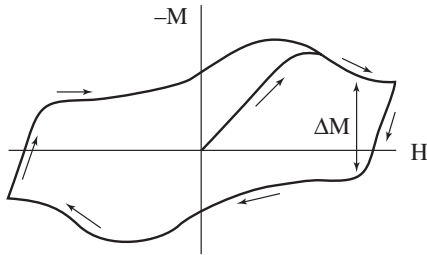


Figure 19.18 - Characteristic magnetization curve of a type-II superconductor

The hysteresis ΔM for a given field is a measure of the critical current density I_c . In equation (19.30), d is the thickness of the sample, or the grain dimension in the case of a polycrystalline ceramic.

The problem of the critical current in type-II superconductors is therefore a technological problem. It is necessary to create defects that pin vortices. For instance, dislocations favour pinning, but the size of the superconducting units also play a role. Commercially available superconducting wires in fact have a very complicated structure. Some superconductors can withstand a current of the order of $10^7 \text{ A} \cdot \text{cm}^{-2}$. Comparing this current density to the maximum density a copper wire can withstand, viz of the order of $10^3 \text{ A} \cdot \text{cm}^{-2}$, we understand the interest of these materials.

field is applied parallel to the hard axis of magnetization, the magnetization is rotated, in a reversible fashion, away from the easy direction. Up until saturation is reached, for $H_{\text{sat}} = 2K_u/M_s$, the magnetization varies linearly with the field according to the law: $M = M_s^2 H / 2K_u$. In this case, magnetization processes involve the continuous rotation of magnetization from positive to negative saturation.

Anisotropic magnetoresistance (AMR) has the form shown in figure 20.15, depending on the relative direction of the current and the field with respect to the easy and hard axes of magnetization. In thin films, the relative amplitude of the AMR decreases for thicknesses of less than about 50 nm due to the increased importance of the scattering of electrons by the external surfaces. The AMR phenomenon has been exploited from 1990 to 1998 in magnetoresistive read heads used to read high storage density computer hard disks (at densities between 0.2 and 2 Gbit.cm⁻²), and is still used nowadays in other types of magnetic field sensors (see ref. [40] and § 6.6 of this chapter).

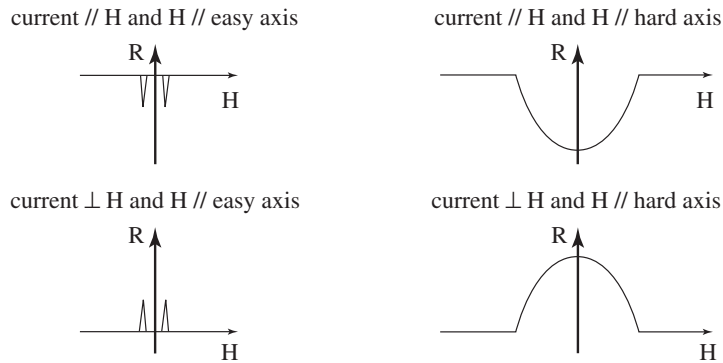


Figure 20.15 - Schematic representation of the anisotropic magnetoresistance of a ferromagnetic thin film having a well defined uniaxial anisotropy

5.3.2. Giant magnetoresistance (GMR)

The giant magnetoresistive effect was discovered in 1988 in (Fe 3 nm/Cr 0.9 nm)₆₀ multilayers [41]. In fact, two remarkable properties were observed in these systems.

The first is the existence of an antiferromagnetic coupling between the Fe layers across the Cr spacer layers (see § 4). For particular intervals of Cr thickness, this coupling tends to align the magnetization of successive Fe films in an antiparallel configuration in zero magnetic field. When a magnetic field is applied in the plane of the structure, the magnetic moments rotate towards the field direction until they become parallel at saturation.

The second remarkable observation made on these multilayers is that the change in the relative direction of the magnetization of the successive Fe films is accompanied by a significant decrease in the electrical resistivity of the structure as illustrated in figure 20.16.

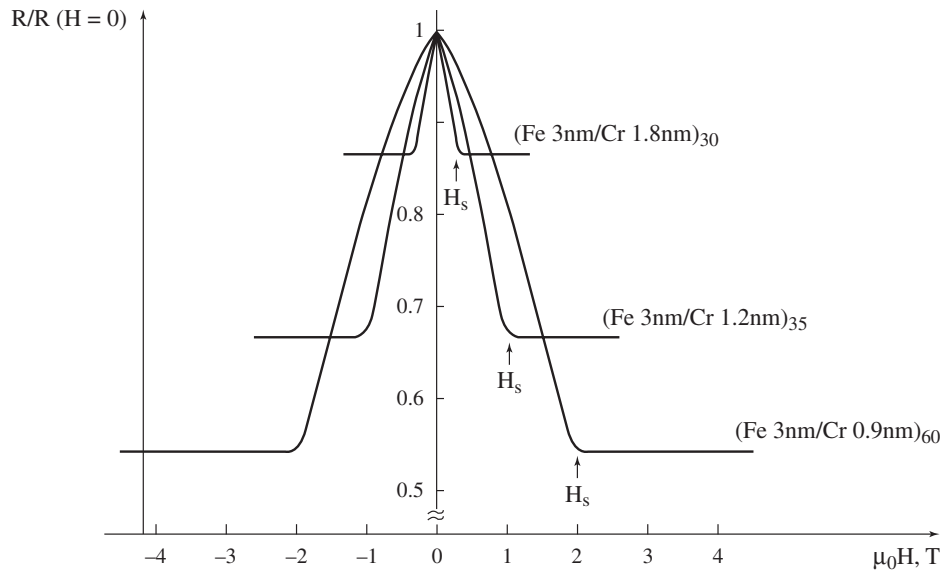


Figure 20.16 - Normalised resistance as a function of the magnetic field

Results observed at $T = 4\text{ K}$ for various (Fe/Cr) multilayers coupled antiferromagnetically, after [41]. The current and magnetic field are parallel to the plane of the film.

Since this first observation, giant magnetoresistive effects have been observed in a number of other systems of the form $B t_B / n^*(F t_F / NM t_{NM}) / C t_C$ where B is a buffer layer chosen to promote the growth of the given structure, n, is the repeat number of basic (F/NM) bilayers, F denotes a ferromagnetic transition metal (Fe, Co, Ni, and most of their alloys), NM a non-magnetic metal which is a good conductor (transition metals: V, Cr, Nb, Mo, Ru, Re, Os, Ir, or noble metals: Cu, Ag, Au...), and t_x represents the thickness of the film x ($x = B, F$ or NM).

The amplitude of the giant magnetoresistance depends very much on the choice of materials used (F, NM), and on the thicknesses of the different layers. It varies from 0.1% in multilayers based on V or Mo to more than 100% in (Fe/Cr) [41, 42] or (Co/Cu) [43, 44] multilayers. In all these structures, it has been observed that the giant magnetoresistance is associated with a change in the relative orientation of the magnetization of successive magnetic layers [41, 45].

Two principal parameters are used to quantify giant magnetoresistance. The first is the GMR amplitude, often defined as $\Delta R / R = (R - R_{\text{sat}}) / R_{\text{sat}}$, where R_{sat} is the resistance at saturation, i.e. the resistance measured when the magnetic moments are aligned parallel. The second is the variation in magnetic field ΔH needed to observe the full GMR value. For many applications, the figure of merit of a material is the ratio $(\Delta R / R) / H_{\text{sat}}$.

indeed large with respect to the gap thickness, as in figure 21.4. This remains true in the most recent products, the *integrated planar* heads (fig. 21.6) [25].

In the so-called *vertical thin film* heads [14, 27], which appeared in the '80s, the magnetic circuit consists of soft magnetic films, which come near the medium in a plane perpendicular to the track, and whose thickness is not much larger than that of the gap (fig. 21.7). Karlqvist's model is clearly less adequate in this case. Calculations suited for this geometry were published as early as 1963 [28]. Numerical methods were also used (see for example ref. [26] for a well-documented review).

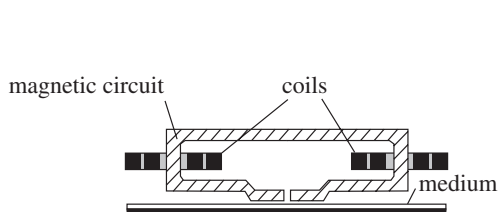


Figure 21.6

Principle of an integrated planar head

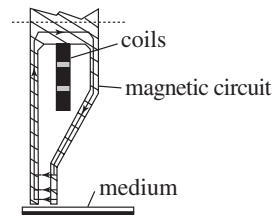


Figure 21.7

Principle of a "vertical thin film" head

Many models assume the permeability of the magnetic circuit to be infinite, or at least homogeneous and isotropic, and restrict the calculation to the static case. In more thorough models, where the ultimate limits are explored, in particular for thin film and integrated planar heads, sophistication is pushed far beyond the mere account of a finite homogeneous and isotropic permeability. This assumption is in fact not justified when the domain size is of the same order as the geometrical dimensions of the problem. The domain structure in the films must then be explicitly taken into account to determine (numerically) the response, which must furthermore be calculated in the dynamic regime. The reader can look up chapter 17 of the present book for more information on dynamic effects, and in particular the frequency dependence of response in a sinusoidal regime.

4.2. STABILITY OF WRITTEN MAGNETIZATION PATTERNS

The above section dealt with the shape of the field produced by the head, and we will later use these results to describe, at least in a semi-quantitative way, the write process. However, before tackling this problem, we investigate the conditions under which a *given* magnetization distribution in the film remains stable in the absence of a write field. This is one aspect of the basic problem of remanence stability, to be compared with the somewhat different view treated in section 3.1.2 of this chapter.

We define in a somewhat arbitrary way a standard distribution of magnetization, representative of those effectively encountered in written media:

$$M_x = M = (2/\pi) M_s \tan^{-1}(x/a) \quad (21.10)$$

This *inverse tangent* distribution corresponds to an isolated transition from the saturated state with $M_x = -M_s$ to the saturated state with $M_x = +M_s$.

Here, Ox of course remains the axis parallel to the track, and we assume \mathbf{M} to depend neither on coordinate z along the width of the track, nor on coordinate y along the medium thickness. We also neglect the perpendicular component M_y of \mathbf{M} . The quantity $2a$ can be considered as the *length* of the transition.

This variation in magnetization produces a pole density $\rho = -\text{div}(\mathbf{M}) = -dM/dx$ which is, in turn, responsible for a demagnetising field \mathbf{H}_d .

We can assume the thickness h of the magnetic film to remain very small with respect to the transition length $2a$. This approximation is not mandatory, but it simplifies the calculations, it is consistent with the assumption on the uniformity of $M(x)$ vs thickness, and it remains realistic enough.

The magnetic film then reduces to the plane Oxz carrying a *surface* distribution of magnetic masses, with density $-h(dM_x/dx)$. We then have:

$$2\pi(x-x')dH_d = -\left(\frac{2M_s h}{a\pi}\right)\left(\frac{dx'}{1+(x'/a)^2}\right) \quad (21.11)$$

Gauss's theorem is here used to express the elementary field produced at x by a line of magnetic masses, with linear density $-h(dM/dx')$, placed at x' . We note that this field has only one component, along Ox. We obtain:

$$H_d = -\frac{M_s h}{\pi^2 a} \int_{-\infty}^{+\infty} \frac{dx'}{(x-x')(1+(x'/a)^2)} \quad (21.12)$$

which, after some simple transformations, gives:

$$H_d = -\left(\frac{M_s h}{\pi a}\right)\left(\frac{x/a}{1+(x/a)^2}\right) \quad (21.13)$$

We see that the demagnetising field is zero at $x = 0$, i.e. at the middle of the transition. It is maximum, equal to $\pm(1/2)(M_s h/\pi a)$, for $x = \pm a$, respectively. If H_C is the coercive field of the material, the stability criterion is simply expressed as $(1/2)(M_s h/\pi a_0) = H_C$, hence:

$$2a_0 = M_s h/\pi H_C \quad (21.14)$$

The *minimum* length of a *stable* transition is thus proportional to the spontaneous magnetization in the material, to the film thickness and to the reciprocal of its coercivity. Increasing the maximum density of bits (which is of the order of $1/2 a_0$) thus requires either decreasing $M_s h$ or increasing H_C . However, as we will see later, it is not advisable to decrease $M_s h$, because this leads to a decrease in the read signal. This is why the improvements now considered for the materials bear mainly on the increase of the coercive field. We recall that formula (21.14) is based on the approximation $2a_0 \gg h$, which implies $H_C \ll M_s/\pi$. If H_C becomes comparable to

M_s then a more exact calculation must be performed [14]. This leads, still under the assumption of a one-dimensional distribution of magnetization, to the conclusion that the transition can become infinitely steep provided $H_C \geq M_s$.

Another approach to evaluating the maximum density of stable bits in a medium starts from the assumption of a *sine-shaped* magnetization profile. The demagnetising field is again easy to calculate, as it was in the inverse tangent distribution we discussed above. The difference is that here we deal with the *magnetostatic* interaction *between bits*, and not just with the demagnetising effect of a single isolated transition. Let p be the period of the distribution (with $p \gg h$), and $K = 2\pi/p$, so that:

$$M_x = M = M_s \sin(Kx) \quad (21.15)$$

We then find:

$$H_d = -(1/2) K M_s h \sin(Kx) = -(1/2) K h M \quad (21.16)$$

Applying the stability criterion $H_d = H_C$ leads to a minimum period p equal to:

$$p = 2\pi/K = M_s h / \pi H_C \quad (21.17)$$

This period should be compared to twice the length of the isolated transition, viz: $4a_0 = 2M_s h / \pi H_C$. We see that p is smaller by a factor two than $4a_0$, which practically means that a succession of transitions is more stable than a single isolated transition. This effect comes from the magnetostatic interaction between bits. A conservative value of the ultimate transition density will thus be: $1/2 a_0 = \pi H_C / M_s h$.

4.3. WRITING A TRANSITION WITH A KARLQVIST HEAD

We just investigated the stability of a transition without asking how it was written. This allowed us in particular to determine the minimum length of this transition.

In a way, this length sets an ultimate limit, which depends only on the coercivity of the recording medium. However, we may also suspect the existence of another limit, possibly a more restrictive one, resulting from the write process itself. We now analyse this write process by considering that the medium remains fixed and that the head moves (fig. 21.8): let x be the coordinate linked to the track, u that linked to the head. The head, constantly fed with the nominal write current I , is moved from left to right on the track, which is initially magnetised in the negative direction. The write field is assumed to be positive, it thus tends to reverse the existing magnetization.

If the write current is large enough, we understand that moving the head produces a magnetization reversal front, *stationary with respect to the head*, near the leading edge of the gap. Behind the head, magnetization has flipped over by 180° .

In a first, very crude approximation, we can neglect the demagnetising field, hence assume that the material is only submitted to the *field from the head*, given by equation (2.1.8) with a change of x for u . Knowing the hysteresis loop of the material, we can then deduce the magnetization profile $M(u)$ in the transition, at least if dynamic

magnetic fluids for use in brakes and clutches were prepared using powdered iron in oil, the particles being of the order of μm or more. Such liquids are, however, unstable (the particles either sink or agglomerate), and when a magnetic field is applied they solidify. Only in the 1960s did the knowledge of how to make what are called stable ferrofluids, using particles 3 to 15 nm in size, become available. They remain liquid even when subjected to intense magnetic fields, and display a magnetic susceptibility sufficiently strong for them to behave like magnetic liquids.

This chapter offers a general outline of these materials, their properties, and their applications. For further information the reader may refer to a very thorough work of reference by R.E. Rosensweig [3], as well as to an article that appeared in French in the journal *La Recherche* [4], which offers an excellent presentation of ferrofluids and contains a more specialised bibliography. Finally, every three years since 1983 the proceedings of the "International Conference on Ferrofluids" [5] have given a very comprehensive list of publications on ferrofluids, as much on the fundamental as on applied aspects, and patents. The volumes for the years 1993 and 1995, in particular, contain review articles concerned with applications.

2. CHARACTERISTICS OF A FERROFLUID

As has been stated, a ferrofluid is composed of small magnetic particles suspended in a carrier liquid.

2.1. STABILITY

One of the characteristics of a good ferrofluid is its stability:

- ◆ stability vis-à-vis gravitational forces: the particles must not settle,
- ◆ stability vis-à-vis magnetic field gradients: the particles must not cluster in regions where the field is intense,
- ◆ stability vis-à-vis the agglomeration of particles under the effect of dipolar forces or Van der Waals type interactions.

The necessary conditions for this stability lead first to a criterion regarding the size of the particles. They must be sufficiently small for the thermal agitation, the brownian motion of the particles, to oppose settling or concentration in a magnetic field gradient. One can obtain an order of magnitude for the acceptable size of particles by comparing the energy terms in play: thermal energy: $k_B T$, gravitational energy: $\Delta\rho V g l$, magnetic energy: $\mu_0 M_p H V$, where k_B is the Boltzmann constant, T the absolute temperature, $\Delta\rho$ the difference in density between the particles and the liquid, V the volume of the particles, g the acceleration of gravity, l the height of liquid in the gravitational field, μ_0 the permeability of free space, M_p the magnetization of the particles and H the magnetic field.

The criterion for stability with regard to gravitational forces is obtained by writing:

$$k_B T / (\Delta \rho V g l) \geq 1 \quad (22.1)$$

Assuming spherical particles of diameter d , a $\Delta \rho$ of $4,300 \text{ kg} \cdot \text{m}^{-3}$ (typical of magnetite Fe_3O_4), a container 0.05 m in height, and a temperature of 300 K, one obtains $d \leq 15 \text{ nm}$.

To estimate the size of the particles that ensure stability in the presence of a field gradient, it is assumed that the magnetic energy $\mu_0 M_p H V$ corresponds to the work performed to move a particle of magnetization M_p in the fluid, from a region where the field has a value H to a region where the field is zero. One then has:

$$k_B T / (\mu_0 M_p H V) \geq 1 \quad (22.2)$$

Taking a magnetization of $4.46 \times 10^5 \text{ A} \cdot \text{m}^{-1}$ (5,600 G, the value for magnetite), and a maximum field of $8 \times 10^4 \text{ A} \cdot \text{m}^{-1}$ (0.1 T), one obtains $d \leq 6 \text{ nm}$.

The stability in field gradients thus seems to be the more demanding factor, leading to particles of size less than 10 nm. These criteria for stability assume that the particles remain small, in other words that they do not agglomerate. But these are small dipoles, and the dipolar interactions tend to cause them to agglomerate. In the same way, at very short distances the Van der Waals force between particles is attractive. The thermal energy needed to oppose the agglomeration of dipolar origin has the same order of magnitude as that which opposes sedimentation. However, agglomeration of Van der Waals origin is irreversible since the energy required to separate two particles, once agglomerated, is very large. Consequently it is necessary to find a way of preventing the particles from getting too close to each other. This can be done:

- ◆ either be coating the particles with a polymer layer to isolate one from the other. These are surfacted ferrofluids, the polymer in question being a surfactant.
- ◆ or by electrically charging the particles, which will then repel because of the Coulomb interaction: these are the ionic ferrofluids.

2.2. TYPES OF FERROFLUIDS AND THEIR PRODUCTION

2.2.1. Surfacted ferrofluids

The surfactant is made up of polymer chains analogous to soap molecules, one end of which adsorbs on the surface of the magnetic particles while the other end has an affinity with the carrier liquid. The particles are thus coated with a layer of polymer which keeps them a certain distance apart. This type of ferrofluid is obtained by milling a coarse powder, generally of magnetite (the grains being of the order of μm in size), in the presence of the surfactant. This operation can take a very long time, up to 1,000 hours. It is the presence of the surfactant during the milling process that makes such a large reduction in size (down to 10 nm) possible, and which results in each grain being covered by a single polymer layer. Using this method it is possible to use

The expression (23.28) now takes the form:

$$\mathbf{B}(\mathbf{r}) = (B_0 + G_X X + G_Y Y + G_Z Z) \mathbf{1}_Z \quad (23.30)$$

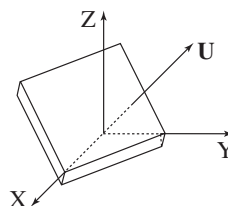
The amplitude of the gradients G_X , G_Y , G_Z , must be adjustable and amenable to modulation in time. A gradient is, of course, expressed in $T \cdot m^{-1}$, but one can also use the unit $Hz \cdot m^{-1}$ if one recalls the relation $F = \gamma B / 2\pi$. In practice the order of magnitude of the gradients used in clinical imaging is of the order of $10 \text{ mT} \cdot m^{-1}$. The relation (23.28) shows that the precession frequencies vary spatially according to the law:

$$f(\mathbf{r}) = f_0 + \gamma \mathbf{G} \cdot \mathbf{r} / 2\pi \quad (23.31)$$

2.3. EXCITATION OF A SYSTEM OF SPINS IN THE PRESENCE OF A GRADIENT: SLICE SELECTION

Here we shall consider samples containing one type of molecule "visible" by NMR (water for example). The process of slice selection is aimed at producing a transverse magnetization in a well defined region of the space. Ideally this region should be limited by two planes, normal to a given direction \mathbf{U} , of the laboratory frame of reference (see fig. 23.15). The distance e between the two planes defines the thickness of the slice. The excitation of the spins contained in a slice of the material normal to \mathbf{U} , and with a thickness e , is effected naturally with the help of selective pulses.

Figure 23.15 - Slice selection



Let us consider a homogeneous material, placed in a field gradient G_X , and let us apply a selective pulse (a sinc or a gaussian for example). Let ΔF be the frequency width over which the pulse is effective (the width at half height of the frequency response $M_{\perp}(F)$). Since $F = F_0 + \gamma G_X X / 2\pi$, the thickness of the slice e is related to the intensity of the gradient by the relation:

$$e = 2\pi \Delta F / \gamma G_X \quad (23.32)$$

One also has:

$$F = F_0 + \gamma G_X X / 2\pi \quad (23.33)$$

The centre of the excited region (i.e. the position of the centre of the slice), X_t , is at $F = F_{rf}$, thus

$$X_t = (F_{rf} - F_0) / 2\pi \gamma G_x \quad (23.34)$$

The adjustment procedure for the slice selection is contained in the relations (23.32) and (23.34) and illustrated in figure 23.16. The frequency width ΔF is fixed from the moment the selective pulse is decided upon (its form, amplitude, duration). *The choice*

of the slice thickness e determines the intensity of the gradient (relation 23.32), while the position of the slice X_t is adjusted by manipulating the frequency of the rotating field F_{rf} (relation 23.34). Due to variations of the signal phase within the body of the slice, it is necessary to reverse the gradient for a time of the order of the half-width of the pulse, after its application.

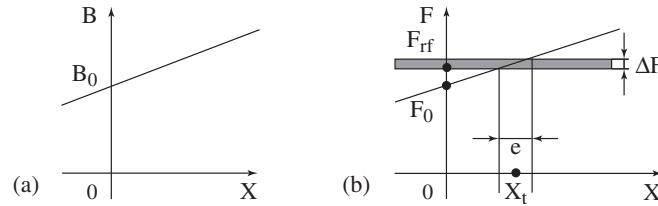


Figure 23.16 - Gradient X: Spatial variation of (a) the magnetic field (b) the Larmor frequency in the laboratory frame of reference

2.4 IMAGING: THE RECIPROCAL SPACE

When the longitudinal magnetization in a three dimensional sample is perturbed by a spatially selective pulse, which is assumed to be applied in the presence of a field gradient G_X (fig. 23.17), the transverse magnetization produced by the selective pulse comes from a Y, Z "plane". The coordinate X_t of this plane depends on the frequency of the pulse. An imaging method should allow determination of the intensity of this magnetization at each point of the plane.

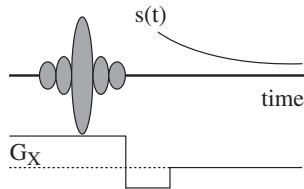


Figure 23.17 - Relative timing of the radiofrequency pulse and the inversion of the gradient G_x during the slice selective excitation
 $s(t)$ represents the NMR signal from the slice.

If the influence of the transverse relaxation is neglected, then the signal at time t_0 , in a homogeneous static field determined by the slice-selection process (see fig. 23.17), is given by:

$$s(t_0) \sim \exp(j2\pi f_0 t_0) \int \rho(Y, Z) dYdZ \quad (23.35)$$

where $\rho(Y, Z)$ is the density of spins at the point X_t , Y, Z, and f_0 the Larmor frequency (in the absence of a gradient, and after a change of frequency). As the magnetic field is assumed to be homogeneous within the slice, f_0 does not depend on the position.

Let us now introduce a gradient pulse in the Y direction, before the acquisition of the signal (fig. 23.18). During this pulse the field is given by $B = B_0 + G_Y Y$. From this one deduces:

$$F = F_0 + \gamma G_Y Y / 2\pi \quad (23.36)$$

resistivity varies from 10 to $10^4 \Omega \cdot m$. The determination of the resistivity at depth by the study of these currents is known as the magnetotelluric method.

The environment can be affected by artificial magnetic fields. On the ground beneath high-tension lines the alternating magnetic field (50 Hz) is of the same order as the local geomagnetic field (10 μT). The biological effects of such alternating fields remain controversial. The electrical current of a lightning strike causes as much damage by the field impulse that it produces, and the associated induction in electrical circuits, as the direct passage of the lightning current into facilities. The enormous amplification of these phenomena in the “fire-ball” of an atmospheric nuclear explosion, capable of destroying by overvoltage the electrical installations over a very extended area, is a very potent weapon that is part of electromagnetic warfare.

7. THE ANCIENT FIELD RECORDED BY PALAEO-MAGNETISM

A knowledge of the past geomagnetic field is possible using palaeomagnetism, provided that the reliability criteria mentioned previously in § 5.1 are fulfilled, that the age of the acquisition of the NRM is known, and that the magnetised object has not been subsequently displaced (in the case of a directional study). The secular variation curve from the Roman period onwards, established by E. Thellier, and shown in figure 24.8, was constructed by measuring the TRM of well dated archaeological baked clays (oven walls, *in situ* fired bricks, etc.) which were collected from all over France. It can be seen that the secular variation during the last two millennia is not the cyclic phenomenon suggested by the historical measurements, which give the impression of a secular variation due to the precession of an inclined dipole. Apart from this chaotic aspect, the average field can be seen to be statistically indistinguishable from the theoretical field calculated for a central axial dipole.

This agreement, which could be fortuitous, is seen to be true for each part of the globe where there are sufficient palaeomagnetic data from volcanic rocks of the last few Ma. Volcanic rocks are used because their ChRM is acquired in less than a year, and therefore it does not risk being filtered by the secular variation, as is the case with sediments. If the field at our scale is non-dipolar with its complex variations, it appears at the scale of 10^3 - 10^6 years as essentially composed of a central axial dipole together with a random noise causing an angular dispersion which varies according to the latitude from 15 to 20° [16]. This stable state characterises the major part of geological time, but sometimes instabilities occur whose amplitudes are much greater than the secular variation. This is called an excursion, as occurred approximately 40 ka ago and lasted of the order 1 ka, when rocks recorded field directions that were practically opposed to those of the actual dipole field.

However, the major instability of the geomagnetic field is its reversal. Palaeomagnetic studies show that the earth's dipole has reversed very many times during the

geological past, and the last occurred 0.78 Ma ago (fig. 24.10). The observation of reversed magnetization in ancient rocks, reported for the first time by Bruhnes at the beginning of the twentieth century in lava flows from Cantal, in the French Massif Central, can only exceptionally be explained by the phenomenon of self reversal invoked by L. Néel (see § 5.1). The process of reversal itself lasts only a few thousand years. On the other hand the average duration of periods where the axial dipole remains pointing to the south (present day state, called normal polarity) or to the north (reversed polarity) is 0.3 Ma for the last 5 Ma.

This process is not cyclic: it obeys Poisson statistics. The elaboration of the geomagnetic reversal time scale (fig. 24.10-b) is based on the compilation of the polarities found in well-dated rocks, and on the use of the magnetic anomalies of the oceanic crust. The reversal sequence can be recovered as a function of the distance from the dorsal axis where the oceanic crust is formed (fig. 24.10-c), or as a function of depth in a sedimentary sequence (fig. 24.10-a).

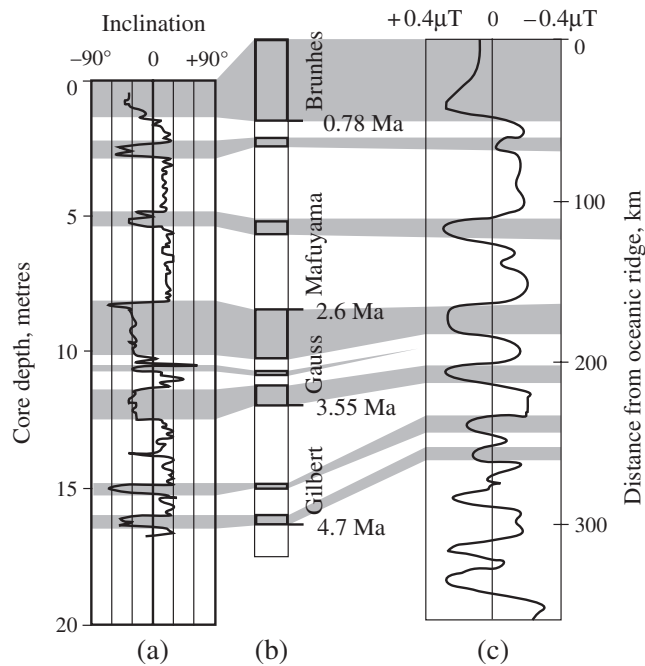


Figure 24.10 - Reversals of the Geomagnetic field

- (a) Record of the inclination of ChRM as a function of the depth in a sediment core from the southern Indian Ocean (inclination of -30° for normal polarity, present day) correlated to the scale in (b);
- (b) Geomagnetic reversal time scale for the last 5 Ma showing the succession of normal periods (in grey as the present day) and reversed (white);
- (c) Geomagnetic field anomalies measured on the surface of the Indian Ocean as a function of the distance from the oceanic ridge and correlated with the reference scale shown in (b).

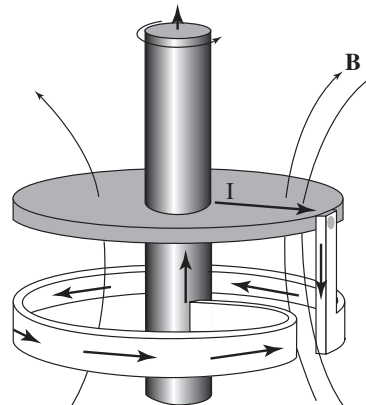
This polarity scale is reliable up to 180 Ma (age of the oldest oceanic crust). Palaeomagnetic studies of continental rocks indicate that before this time the geomagnetic field had similar characteristics. However, there were long periods without reversals known as quiet intervals or superchrons (Permian reversed period between 312 and 262 Ma, and the Cretaceous normal from 118 to 83 Ma).

From the point of view of its intensity the geomagnetic field also shows large variations, both during stable periods (for example g_{10} was 30% greater 3 ka ago) as well as during excursions or reversals (reduction by a factor of 5 to 10). This fact as well as the recordings of the same event at different points around the globe, seems to prove that during excursions and reversals there is a temporary disappearance of the dipole field, and that it does not undergo a progressive rotation by 180° .

8. ORIGIN OF THE CORE FIELD: DYNAMO THEORY

The possibility of maintaining a permanent magnetic field by the transformation of mechanical energy into a self-excited field-current system is termed the dynamo effect. A very simple laboratory device, the disc dynamo, can show these properties: it consists of a conducting disc rotating in a field \mathbf{B} so inducing a current I that is fed into a conducting loop. This creates a field that reinforces the original field. Above a certain critical rotational velocity, one can remove the initial external field, and so produce a self-excited field. Moreover, for the same set up and sense of rotation two polarities of the field are possible (fig. 24.11). This is quite similar to the behavior of the geomagnetic field, which can exhibit two opposite “stationary” states.

Figure 24.11
Example of a machine capable of producing a self-excited magnetic field
A conducting disc (shaded) rotates in a magnetic field \mathbf{B} with an angular velocity ω . The induced current I in the disc flows in a fixed circuit (unshaded) in the form of a loop which produces a magnetic field in the same sense as the initial field \mathbf{B} .



Obviously the processes occurring in the outer core (conducting liquid, with a temperature in its upper part of around 3,000 K and a viscosity similar to that of water, figure 24.12-a) are eminently more complex than that of a simple disc dynamo, and a serious description of the actual theory of the earth's dynamo is well beyond the scope of this book [10, 14, 16]. In order to compensate for ohmic dissipation, energy

3.2. MAGNETIC MANIPULATION OF CATHETERS

An increasing number of surgical operations call on microsurgery techniques, which in their preliminary phase require a micro-instrument to be directed towards the site of the intervention. Generally, this micro-instrument is carried by a catheter that passes along the blood vessels; but at a bifurcation, it can happen that the catheter obstinately takes the wrong path.

It is then impossible to carry out the operation, and the patient could die: this is why, as from 1951, the technique of magnetic guidance of intravascular catheters was developed under the leadership of Tillander in Sweden [14]. The first applications only concerned those vessels that were sufficiently large to admit these devices, which were at that time quite bulky: aorta, renal and pancreatic arteries.

The technique is still the same: a magnet is fixed to the end of a flexible catheter. During the progression of the catheter along the artery or vein of the patient, should the catheter try to take the incorrect route, then the application of an ad hoc magnetic field gradient will deviate the extremity of the catheter towards the correct direction and allow the micro-instrument to continue its progress towards the target.

This remarkable technique has continued to progress, in particular with the appearance of magnets of much higher energy density so that the same result is achieved for a considerably reduced volume.

Such progress has since allowed this technique to be applied to neurosurgery: for example in the case of the treatment of aneurysms, A. Lacaze (CNRS Grenoble) developed a magnetic guidance system which takes advantage of the remarkable properties of modern samarium-cobalt magnets.

Figure 25.4 illustrates the principles of this technique: the catheter C should reach the aneurysm A, but it has a tendency to pass into the vein B1. A strong mini-magnet M under the influence of a field gradient in the direction of the arrow H attracts the catheter into the vein B2, then by reversing the field gradient, into the aneurysm A.

This magnetic guidance technique is used in a number of different operations, because it is less invasive than classic surgical techniques and avoids the necessity of making large incisions which take longer to heal: for example the treatment of varicose veins can now be carried out from inside the veins, without having to perform multiple incisions along the length of the vein.

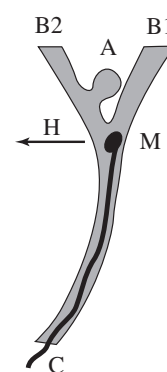


Figure 25.4
Aneurysm therapy

Aperiodic displacement of the sample and measurement by an RF (radiofrequency) SQUID

Sensitivity: 10^{-9} to 10^{-11} A. m²

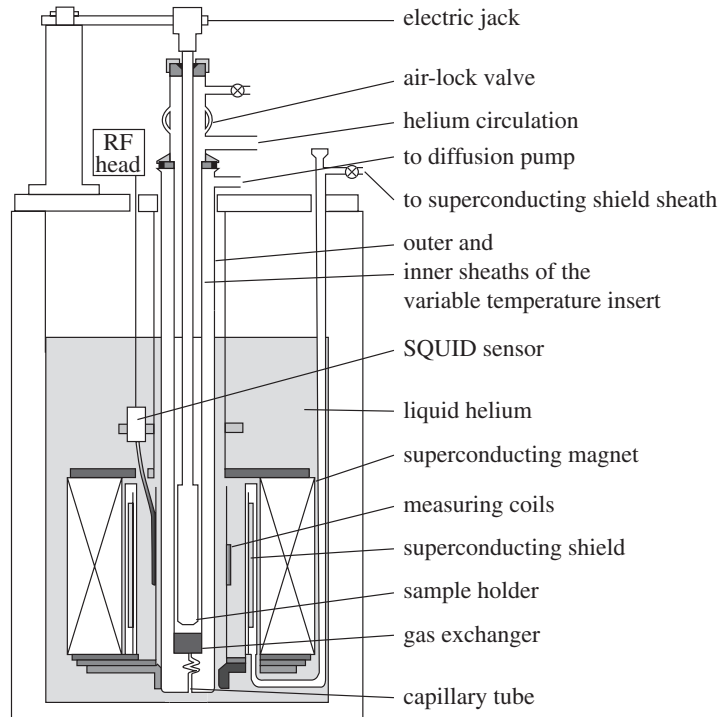


Figure 26.10 - Diagram of an 8 teslas RF SQUID magnetometer with variable temperature ($1.5 < T < 300$ K)

A parallel resonant R, L, C circuit (fig. 26.11-b) is fed at its resonant frequency $\omega/2\pi$ (chosen between 10 and 300 MHz) by a current $i = I_{RF} \sin \omega t$. The current that flows in the inductance is $Q i$ ($Q = L\omega/R$ is the quality factor, R being the resistance of the inductance), and the peak voltage across this circuit is: $V_t \approx QL\omega I_{RF}$.

A small superconducting ring, interrupted by a Josephson junction, is now placed close to the previous circuit, and coupled to the inductance L by a mutual inductance M' . A Josephson junction can be an insulating gate of the order of a nanometer in thickness. Josephson showed that phase coherence between Cooper pairs (that are at the origin of superconductivity) persists through such a gate. The interest of the Josephson junction is to lower the critical current i_c of the ring to a few microamperes. The critical flux ϕ_c of the ring $\phi_c = L_s i_c$, where L_s is the inductance of the ring, is then a few flux quanta (a flux quantum is $\phi_0 = 2.07 \times 10^{-15}$ weber).

One sees that the characteristic $V_t(I_{RF})$ is no longer a straight line. Due to the presence of the ring, the current $Q i$ that flows in the inductance induces in the ring an AC flux of amplitude:

$$\phi_1 = M' Q I_{RF} \quad (26.13)$$

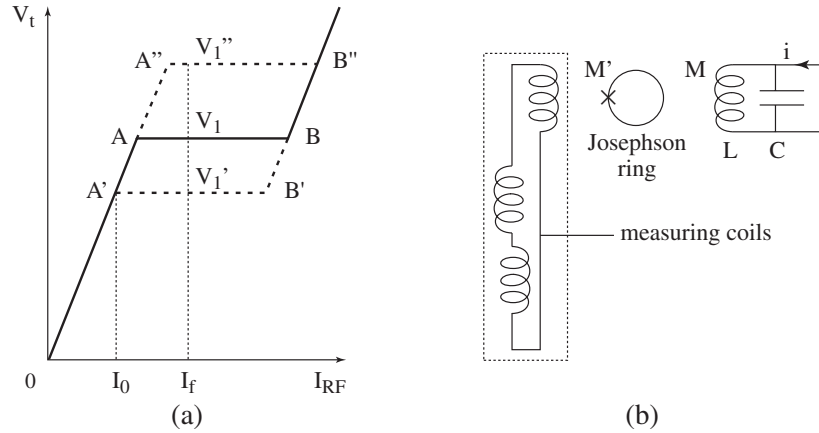


**Figure 26.11 - (a) Ideal voltage-current characteristic of an RF SQUID
(b) Circuit diagram of a SQUID sensor**

When ϕ_1 reaches ϕ_c (for a current $I_0 = \phi_c / M' Q$ –corresponding to point A on the characteristic of figure 26.11-a) or exceeds it, there occurs a periodic admission of a flux quantum flux ϕ_0 , followed by the expulsion of this flux quantum $(2n + 1) \pi / \omega$ later, where n is an integer which is larger the closer one is to point A.

The voltage across the resonant circuit becomes constant (plateau AB), and equal to:

$$V_T = Q L \omega I_0 \quad (26.14)$$

The end of the plateau, point B on figure 26.11-a, occurs when the admission and expulsion of a flux quantum occur every half-cycle of the current, that is at intervals of π / ω . One chooses an operating current I_f near the middle of the plateau AB. A DC flux $\delta\phi$ is now superimposed on the AC flux: the plateau on the characteristic is reached when the total maximum flux $\phi_1 + \delta\phi$ reaches the value ϕ_c . It occurs earlier (A'B') or later (A''B'') for a current $I_0' = (\phi_c - \delta\phi) / M' Q$.

The variation of voltage $\delta V = Q L \omega (I_0 - I_0')$ corresponds to a variation in flux $\delta\phi = M' Q (I_0 - I_0')$ so that:

$$\delta V = (L \omega / M') \delta\phi \quad (26.15)$$

Thus a *DC flux* \rightarrow *peak voltage* converter has been achieved.

The DC flux is applied using a superconducting circuit consisting of a pick-up coil and a small inductance, coupled to the Josephson ring through a mutual inductance M' (fig. 26.11-b). The pick-up coil consists of two coils connected in series opposition, each of 2 or 3 turns, with their axes parallel to the applied field.

When one displaces the sample in the coils, as in the previously described extraction method, to determine its moment \mathfrak{m} , the variation of flux given by (26.3) is:

$$\delta\phi = \delta(B/I) \mathfrak{m} \quad (26.16)$$

The current variation δi in the superconducting measurement circuit with inductance $\sum L_i$ is then given by:

$$\delta\phi = (\sum L_i) \delta i \tag{26.17}$$

The flux variation seen by the superconducting ring:

$$\delta\phi_2 = M'' \delta i \tag{26.18}$$

is compensated by a feedback flux equal and opposite to $\delta\phi_2$, generated by a current δi_{cr} flowing in the inductance of the resonant circuit $\delta\phi_{cr} = M' \delta i_{cr} = -\delta\phi_2$. From equations (26.16) to (26.18), one obtains the magnetic moment of the sample:

$$m = - \frac{M' (\sum L_i) \delta i_{cr}}{M'' \delta(B/I)} \tag{26.19}$$

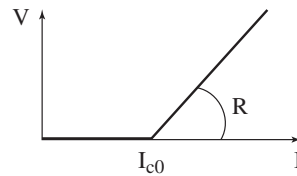
Magnetometers using SQUID sensors are relatively slow because they measure a DC flux. After every magnetic field change, the magnetic field source (almost always a superconducting coil) has a lag, and one must wait until the drift is sufficiently small to be able to make a precise measurement. When measuring in a constant magnetic field, this problem disappears, and the magnetometer has good performance.

DC SQUID detection

A DC SQUID can also be used to convert a change of magnetic flux into a voltage variation.

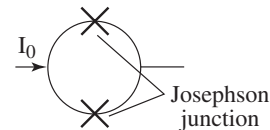
The voltage across a Josephson junction supplied with a direct current I remains zero as long as $I < I_{c0}$, where I_{c0} is the critical current of the junction. For greater currents one observes a voltage $V \approx R (I - I_{c0})$ (fig. 26.12), R being the equivalent resistance of the junction.

Figure 26.12
Ideal characteristic of a Josephson junction



A DC SQUID is made up of a superconducting loop broken by 2 Josephson junctions each having a critical current I_{c0} (fig. 26.13).

Figure 26.13 - Diagram of a DC SQUID



The loop is fed with a direct *bias* current I_0 slightly greater than $2 I_{c0}$. The voltage across the SQUID is then simply $V = R (I_0 - 2 I_{c0}) / 2$, corresponding to the fact that the SQUID has a critical current $2 I_{c0}$, and an equivalent resistance $R / 2$ (fig. 26.14-a). If one applies a flux $\delta\phi$ to the loop, which has an inductance L , an induced shielding